Optics Letters

Coupled cavity-waveguide based on topological corner state and edge state

Aoqian Shi,[1] Bei Yan,[1] Rui Ge,[1] Jianlan Xie,[1] Yuchen Peng,[1] Hang Li,[1] Wei E. I. Sha,[2] and Jianjun Liu[1,*]

[1]Key Laboratory for Micro/Nano Optoelectronic Devices of Ministry of Education & Hunan Provincial Key Laboratory of Low-dimensional Structural Physics and Devices, School of Physics and Electronics, Hunan University, Changsha 410082, China
[2]State Key Laboratory of Modern Optical Instrumentation, College of Information Science and Electronic Engineering, Zhejiang University, Hangzhou 310027, China
*Corresponding author: jianjun.liu@hnu.edu.cn

Received 5 January 2021; revised 30 January 2021; accepted 31 January 2021; posted 1 February 2021 (Doc. ID 418570); published 24 February 2021

The topological corner state (TCS) and topological edge state (TES) have created new approaches to manipulate the propagation of light. The construction of a topological coupled cavity-waveguide (TCCW) based on the TCS and TES is worth looking forward to, due to its research prospects in realizing high-performance micro-nano integrated photonic devices. In this Letter, the TCCW is proposed in two-dimensional (2D) photonic crystal (PC), which possesses strong optical localization, high quality factor, and excellent robustness compared with the conventional coupled cavity-waveguide (CCCW). This work will pave the way toward designing high-performance logic gates, lasers, filters, and other micro-nano integrated photonics devices and expanding their applications.

https://doi.org/10.1364/OL.418570

Manipulating the propagation of light is the core content in the field of optical communication. With its unique bandgap and local characteristics, photonic crystal (PC) has become an effective carrier for realizing on-chip integrated optical communication [1,2]. A coupled cavity-waveguide (CCW) based on PCs can realize the input, localization, and output of optical signals, and has been widely used in filters [3,4], sensors [5,6], lasers [7,8], and other micro-nano integrated photonics devices. However, the performance of the conventional optical waveguide and optical cavity is easily affected by obstacles and defects caused by actual fabrication errors.

Photonic topological insulators and their topological states have created new materials and new approaches to manipulate the propagation of light. The topological edge state (TES) [9–24] and topological corner state (TCS) [25–32] have been generated based on topological phase transition. The optical waveguide based on the TES (i.e., TES waveguide), without backscattering and immune fabrication errors [9–12], has been applied to splitters [17], logic gates [18], and lasers [21], which significantly improved device performance. The optical cavity based on the TCS (i.e., TCS cavity) can achieve strong localization without introducing defect structures [26], but its application is very limited by its inability to transmit optical signals. If the TCS cavity and TES waveguide are combined, a unique CCW named the topological CCW (TCCW) will be formed, which will be topologically protected. The construction of the TCCW is worth looking forward to, since it possesses both strong localization and robust transmission, and possesses the possibility to design high-performance logic gates, lasers, filters, and other micro-nano integrated photonic devices and expand their applications. Different from the previous CCWs [18,21], which localized the energy within an annular region, this TCCW will localize the optical signal at a point, so as to achieve stronger localization with smaller geometry volume, which will be more conducive to the design of on-chip integrated optical communication devices.

In this Letter, the TES waveguide and the TCS cavity are proposed based on the bulk-edge-corner correspondence of the square lattice PC. Owing to the flat band characteristics of the edge of the TES band and the strong localization of the TCS, the TCCW constructed with the TCS cavity and TES waveguide has strong cavity-waveguide interaction. In contrast to the conventional CCW (CCCW) constructed with a point-defect cavity and line-defect waveguide, the strong optical localization, high quality factor, and excellent robustness of the TCCW are verified by theoretical investigation and numerical simulation.

The lattice constant of the square lattice PC is $a = 0.5$ μm, the initial side length of the square dielectric rod is $l_0 = 0.44a$, the refractive index $n_a = 3.47$, and the background refractive index $n_b = 1$. As shown in Fig. 1(a), the square lattice PC protected by inversion symmetry has four inversion centers, denoted as A, B, C, and D, respectively. As shown in Figs. 1(b) and 1(c), the four inversion centers correspond to four types of the unit cell (UC), respectively. After the periodic array, four types of square lattice PCs can be obtained (only the shapes of scatterers at four boundaries of each PC are not the same). It can be seen from Fig. 1(d) that, although the arrangement of the scatterers in the four UCs is different, their band structures are the same and have a common bandgap. By analyzing the symmetry of the electric field E_z at the Γ and X(Y) points in the

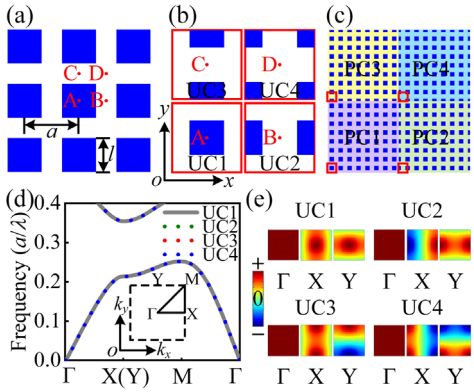

Fig. 1. (a) Square lattice PC. (b) Four types of UC. (c) Four kinds of square lattice PC constructed with periodic arrays of four UCs (red box). (d) The band structures of four UCs under TM polarization, among which the three dotted lines of green, red, and blue overlap, and only the blue dots are shown. (e) The electric field E_z of the four UCs at the high symmetry points of the first bulk band.

Brillouin zone, the corresponding Zak phases can be obtained, as shown in Fig. 1(e).

According to the bulk-edge correspondence, when the Zak phase of the PC bulk bands changes, there will be a TES in the corresponding bandgap [33]. When considering the first bulk band, the Zak phase of the two-dimensional (2D) PC along the j direction is [13,27]

$$\theta_j^{\mathrm{Zak}} = \int \mathrm{d}k_x \mathrm{d}k_y \,\mathrm{Tr}[\mathbf{A}_j(k_x, k_y)],\ j = x, y, \tag{1}$$

where the integral range is the first Brillouin zone, $\mathbf{A}_j(k_x, k_y) = i\langle\psi|\partial_{k_j}|\psi\rangle$ is the Berry connection, and ψ represents the periodic parts of Bloch functions. There is a corresponding relationship between the Zak phase and the 2D polarization ($\mathbf{P}$) along the j direction: $\theta_j^{\mathrm{Zak}} = 2\pi P_j$ [13]. In the structure protected by inversion symmetry, the value of the Zak phase is quantized and can only be 0 or π. In this Letter, the Zak phase is determined by the electric field E_z of the eigenvalues at the high symmetry points in the Brillouin zone. Considering that the electric field E_z at Γ point is mirror symmetric, if the electric field E_z at X(Y) point along the $x(y)$ direction is mirror symmetric/antisymmetric, the Zak phase in this direction is 0 (trivial phase)/π (topological non-trivial phase) [12,27]. It can be seen from Fig. 1(e) that the 2D Zak phases of the four PCs are (0, 0), (π, 0), (0, π), and (π, π) respectively, and the corresponding 2D $\mathbf{P}$ is (0, 0), (1/2, 0), (0, 1/2), and (1/2, 1/2). The Zak phases of the four PCs are different. The reason is that the value of the Zak phase is related to the inversion center (the center of the UC), and the Zak phase difference of the UCs corresponding to the two inversion centers along the j direction is π [33]. For two PCs with a Zak phase difference along the $x(y)$ direction, their combined structure will lead to the TES at the interface along the $y(x)$ direction.

In order to observe the TES, PC1 is combined with PC3 and PC4 along the x direction, respectively, and the projected band structures are calculated as plotted in Figs. 2(a) and 2(b). There are TESs (TES1 and TES2, respectively) in the bandgap of the combined structures. However, the topology of the TESs in Figs. 2(a) and 2(b) is not the same, which is related to edge polarization (p_j^{edge}). Similar to bulk polarization, edge polarization can be determined by the symmetry of the electric field E_z at high symmetry points in the Brillouin zone. From the illustrations in Figs. 22(a) and 2(b), at (0, 0), the electric field E_z of the two TESs are mirror symmetric, and at (π/a, 0), TES1 is mirror symmetric, while TES2 is mirror antisymmetric. Therefore, the two edge polarizations along the x direction are $p_{x(\mathrm{TES1})}^{\mathrm{edge}} = 0$ and $p_{x(\mathrm{TES2})}^{\mathrm{edge}} = 1/2$, respectively. If PC1 is combined with PC3 and PC4, respectively, along the y direction, the former will no longer have TES (i.e., $p_{y(\mathrm{TES1})}^{\mathrm{edge}} = 0$), while the latter will still have TES with $p_{y(\mathrm{TES2})}^{\mathrm{edge}} = 1/2$. The existence of the TCS depends on the edge polarization [34],

$$Q^{\mathrm{corner}} = p_x^{\mathrm{edge}} + p_y^{\mathrm{edge}}. \tag{2}$$

According to Eq. (2), when $p_j^{\mathrm{edge}} = 1/2$, $Q^{\mathrm{corner}} = 1$, which corresponds to the existence of the TCS, while $p_j^{\mathrm{edge}} = 0$ cannot lead to TCS. By calculating the eigenmodes of the combined structure of PC1 and PC4, the existence of TCS can be verified, as depicted in Figs. 2(c) and 2(d).

It can be seen from Fig. 2(c) that there is TCS in the bandgap of the TES, and the corresponding normalized frequency is 0.325. Figure 2(d) shows the electric field E_z of the TCS. The electromagnetic energy is strongly located in the 90° corner formed by the combination of two PCs.

In this Letter, TCCW is constructed with the TCS cavity and TES waveguide. At the same time, the CCCW is constructed with the point-defect cavity and line-defect waveguide. The performances of the two structures are simulated and analyzed, as shown in Fig. 3. The blue part is the TCS cavity in Fig. 3(a), which is constructed with PC1 and PC4, and the side length of the square dielectric rod is $l_c = 0.44a$. The yellow part is the TES waveguide, which is constructed with PC1 and PC3, and the side length of the square dielectric rod is $l_w = 0.386a$. The size of square dielectric rods in TES waveguide is different from that in the TCS cavity to make edge states covering the

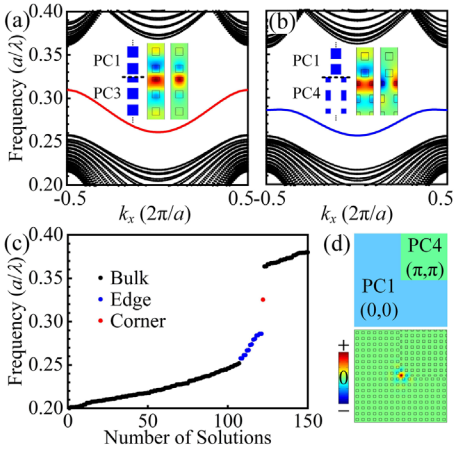

Fig. 2. (a) and (b) The projected band structures of PC1 combined with PC3 and PC4, respectively. The insets show the supercells (15 unit cells for each PC) and electric field E_z of two TESs at the high symmetry points (0, 0) (left) and (π/a, 0) (right). (c) The eigenmodes of the combined structure of PC1 and PC4. (d) The schematic of the combined structure (256 unit cells) of PC1 (192 unit cells) and PC4 (64 unit cells) and the electric field E_z of the TCS.

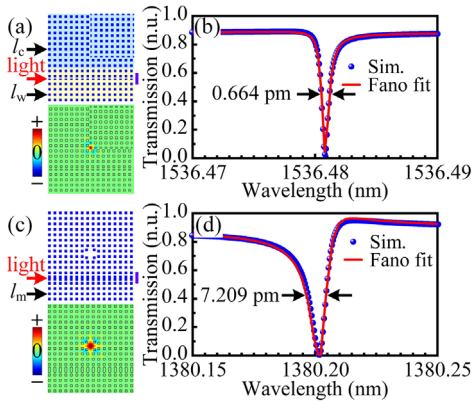

Fig. 3. (a) Schematic of the TCCW (top), the electric field E_z of the resonance mode (bottom). The red arrow and the purple rectangle correspond to the light source and the monitor, respectively. (b) Transmission spectrum: simulated data points and Fano fitting. (c) The schematic of the CCCW (top), and the electric field E_z of the resonance mode (bottom). (d) Transmission spectrum: simulated data points and Fano fitting.

frequency of corner state. In order to make the performance comparison of TCCW and CCCW fairer, a similar structure is adopted for both. The side length of the square dielectric rod of the CCCW is $l_m = 0.4a$. To construct the point-defect cavity of the CCCW, the interval between four adjacent square dielectric rods is expanded from a to $1.4a$. To construct the line-defect waveguide of the CCCW, a row of rectangular dielectric rods with a size of $2.5\ l_m \times l_m$ is introduced, as shown in Fig. 3(c).

The CCW constructed with localization mode cavities and transmission mode waveguides will lead to Fano resonance with the line shape of sharp and asymmetry. The line shape of the Fano resonance can be expressed as [35,36]

$$F(\omega) = A_0 + F_0 \frac{[q + 2(\omega - \omega_0)/\Delta\omega]^2}{1 + [2(\omega - \omega_0)/\Delta\omega]^2}, \tag{3}$$

where A_0 and F_0 are constants, ω_0 is the resonance frequency, $\Delta\omega$ is the resonance linewidth, and q is the Fano parameter, indicating the degree of asymmetry. It can be seen from Figs. 3(b) and 3(d) that the transmission spectrum data points calculated by simulation fit well with the Fano line shape, and the resonance linewidth of the TCCW is much smaller than that of the CCCW, which corresponds to stronger localization.

The quality factor (Q) is an important performance parameter of CCW, which can be expressed by the resonance frequency (ω_0) and the decay time (τ) of the electromagnetic energy in the cavity or the resonance linewidth ($\Delta\omega$) [37] as

$$Q = \frac{\omega_0 \tau}{2} = \frac{\omega_0}{\Delta\omega}, \tag{4}$$

and $Q = 2.3139 \times 10^6$ (1.9144×10^5) of the TCCW (CCCW) can be calculated from Eq. (4).

Next, we further analyze the reasons why both the TCCW and CCCW have high Q and the Q of the TCCW is better than that of the CCCW. The Q in the CCW consists of two parts in time τ, namely the radiation part Q_r to the surrounding environment in time τ_r and the coupling part Q_w to the waveguide in time τ_w. The relationship between the parameters can be expressed as $1/Q = 1/Q_r + 1/Q_w$ and $1/\tau = 1/\tau_r + 1/\tau_w$

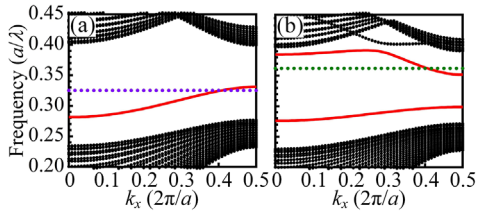

Fig. 4. (a) Projected band structure of the TES waveguide. The purple dotted line corresponds to the frequency of TCS. (b) The projected band structure of the line-defect waveguide, the green dotted line corresponds to the resonance frequency of the point-defect cavity.

[37], where τ_r is determined by the material and geometry of the cavity and can be qualitatively expressed as $\tau_r = f(a, \varepsilon, \delta, N)$, a is the lattice constant, ε is the dielectric constant, δ is the filling rate, and N is the number of lattice periods around the cavity. The τ_w is determined by the material and geometry of the waveguide and the distance (d_{cw}) between the cavity and the waveguide.

The material and geometry of the waveguide determine the dispersion relationship and, thereby, the density of states DOS(ω) of the transmission mode. When the frequency of the transmission mode is equal to the resonance frequency of the cavity, that is, $\omega = \omega_0$, the waveguide mode and the cavity mode are coupled. Considering the DOS(ω_0) at the resonance frequency, its definition is [38]

$$\mathrm{DOS}(\omega_0) = \left(\frac{1}{\pi}\right)\left(\frac{\partial k}{\partial \omega}\right)_{\omega=\omega_0}, \tag{5}$$

where $\partial k/\partial\omega$ is the reciprocal of the slope of the dispersion curve (that is, the reciprocal of the group velocity). DOS(ω_0) represents the number of eigenmodes corresponding to the cavity resonance frequency, and decay time is proportional to it, $\tau_w \propto \mathrm{DOS}(\omega_0)$ [39]. The decay time is proportional to the decay distance, namely $\tau_w \propto d_{cw}$. Consequently, τ_w can be qualitatively expressed as $\tau_w = f(\mathrm{DOS}(\omega_0), d_{cw})$. Considering $Q_r \gg Q_w$ in the CCW [37], it can be deduced from $1/Q = 1/Q_r + 1/Q_w$ that Q mainly depends on Q_w. Under the condition of $d_{cw} = 4a$, DOS(ω_0) of the TCCW and CCCW is compared and discussed as depicted in Fig. 4. As elaborated below, the group velocities corresponding to the resonance frequency of both the TCCW and CCCW are small; that is, the values of $\partial k/\partial\omega$ are large. According to Eq. (5), DOS(ω_0) has large values, which leads to high Q_w; thus, both the TCCW and CCCW have high Q. However, the TCCW has stronger optical localization, which also enhances the interaction between the cavity and waveguide, thus leading to a higher Q than the CCCW.

In addition to strong localization and high Q, the TCCW can also be immune to obstacles and defects caused by actual fabrication errors, which is the main difference between the TCCW and CCCW. To verify this point, the robustness (R) (anti-interference performance) of the TCCW and CCCW is further explored. Under certain external disturbances, R denotes the change of CCW performance parameters, which can be qualitatively expressed as

$$R_{\mathrm{CCW}} = f(\alpha, \beta, s), \tag{6}$$

where $\alpha = \Delta\lambda_0/\lambda_0$, λ_0 is the resonance wavelength, and $\Delta\lambda_0$ is its offset; $\beta = \Delta Q/Q$, Q is the quality factor of the structure,

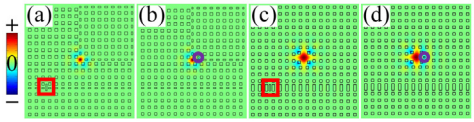

Fig. 5. (a) and (b) TCCW: the resonance wavelengths are 1536.48 nm and 1538.64 nm, respectively, and corresponding Q are 2.2463×10^6 and 1.7698×10^6. (c) and (d) CCCW: the resonance wavelengths are 1380.20 nm and 1363.43 nm, respectively, and corresponding Q are 9.3857×10^4 and 5.8238×10^4. The red rectangle corresponds to the metal obstacle (s_1), and the purple circle corresponds to the defect (s_2).

Table 1. Comparison of Robustness between TCCW and CCCW

CCW	$\alpha(s_1)$	$\beta(s_1)$	$\alpha(s_2)$	$\beta(s_2)$
TCCW	1.6×10^{-6}	2.9%	0.1%	23.5%
CCCW	2.3×10^{-6}	50.9%	1.2%	69.6%

and ΔQ is its offset; s is the interference factor, corresponding to the obstacle, defect, etc.

In this Letter, the R_{CCW} of the TCCW and CCCW are compared in the case of introducing metal obstacle (s_1) in the waveguide and introducing a defect (s_2) of the square dielectric rod with side length of $0.25a$ in the cavity. It can be seen from Figs. 5(a)–5(d) and Table 1 that $\alpha(s_1)$, $\alpha(s_2)$, $\beta(s_1)$, and $\beta(s_2)$ of the TCCW (CCCW) have small (large) changes under the same interference conditions. It should be noted that for side coupling of the cavity and waveguide, there are several lattice periodic intervals between the cavity and waveguide. In this case, the disturbance of the waveguide structure has little effect on the inherent resonance frequency of the cavity [37]; thus, the $\alpha(s_1)$ is small with 10^{-6} orders of magnitude in our CCWs. Although the TCCW is also affected by fabrication errors, its affected degree is far lower than that of the CCCW, which reflects a relatively excellent anti-interference performance. Therefore, the TCCW proposed in this Letter possesses excellent applicability for micro-nano integrated photonic devices that require strong localization, high Q (i.e., narrow linewidth), and stable resonance frequency, such as filters [3,4] and lasers [7,8,21].

In this Letter, TCCW is constructed with a TCS cavity and TES waveguide, and its resonance characteristics and DOS are investigated. In contrast to the CCCW, it is proved that the TCCW possesses strong optical localization, high Q, and excellent robustness, which paves the way toward manipulation of the propagation of light and realizing high-performance micro-nano integrated photonic devices.

Funding. Fundamental Research Funds for the Central Universities (531118040112); Natural Science Foundation of Hunan Province (2017JJ2048, 2020JJ4161); National Natural Science Foundation of China (61405058, 62075059).

Acknowledgment. The authors acknowledge Professor Jian-Qiang Liu for software sponsorship.

Disclosures. The authors declare no conflicts of interest.

REFERENCES

1. E. Yablonovitch, Phys. Rev. Lett. **58**, 2059 (1987).
2. S. John, Phys. Rev. Lett. **58**, 2486 (1987).
3. S. Fan, P. R. Villeneuve, J. D. Joannopoulos, and H. A. Haus, Phys. Rev. Lett. **80**, 960 (1998).
4. A. Dideban, H. Habibiyan, and H. Ghafoorifard, Physica E **87**, 77 (2017).
5. S. H. Mirsadeghi, E. Schelew, and J. F. Young, Appl. Phys. Lett. **102**, 131115 (2013).
6. P. Liu and Y. Shi, Opt. Express **25**, 28398 (2017).
7. Y. Xiong, T. Umeda, X. Zhang, M. Morifuji, H. Kajii, A. Maruta, and M. Kondow, IEEE J. Sel. Top. Quantum Electron. **24**, 4900207 (2018).
8. P. M. Kamiński, S. Arslanagić, J. Mørk, and J. Li, Phys. Rev. A **100**, 053808 (2019).
9. F. D. M. Haldane and S. Raghu, Phys. Rev. Lett. **100**, 013904 (2008).
10. Z. Wang, Y. D. Chong, J. D. Joannopoulos, and M. Soljačić, Phys. Rev. Lett. **100**, 013905 (2008).
11. L. H. Wu and X. Hu, Phys. Rev. Lett. **114**, 223901 (2015).
12. X. Huang, Y. Yang, Z. H. Hang, Z. Q. Zhang, and C. T. Chan, Phys. Rev. B **93**, 085415 (2016).
13. F. Liu and K. Wakabayashi, Phys. Rev. Lett. **118**, 076803 (2017).
14. F. Gao, H. Xue, Z. Yang, K. Lai, Y. Yu, X. Lin, Y. Chong, G. Shvets, and B. Zhang, Nat. Phys. **14**, 140 (2017).
15. X. Chen, D. Zhao, X. Zhu, F. Shi, H. Liu, J. Lu, M. Chen, and J. Dong, Phys. Rev. A **97**, 013831 (2018).
16. C. Ji, G. Liu, Y. Zhang, B. Zou, and Y. Yao, Phys. Rev. A **99**, 043801 (2019).
17. M. Makwana, R. Craster, and S. Guenneau, Opt. Express **27**, 16088 (2019).
18. L. He, W. X. Zhang, and X. D. Zhang, Opt. Express **27**, 25841 (2019).
19. B. Yan, J. Xie, E. Liu, Y. Peng, R. Ge, J. Liu, and S. Wen, Phys. Rev. Appl. **12**, 044004 (2019).
20. Y. Peng, B. Yan, J. Xie, E. Liu, H. Li, R. Ge, F. Gao, and J. Liu, Phys. Status Solidi RRL **14**, 2000202 (2020).
21. Y. Zeng, U. Chattopadhyay, B. Zhu, B. Qiang, J. Li, Y. Jin, L. Li, A. G. Davies, E. H. Linfield, B. Zhang, Y. Chong, and Q. J. Wang, Nature **578**, 246 (2020).
22. Y. Wu, X. Li, and Y. Fang, J. Opt. **22**, 105102 (2020).
23. M. L. N. Chen, L. J. Jiang, Z. Lan, and W. E. I. Sha, Phys. Rev. Res. **2**, 043148 (2020).
24. Z. Lan, J. W. You, Q. Ren, W. E. I. Sha, and N. C. Panoiu, "Second harmonic generation via double topological valley-Hall kink modes in all-dielectric photonic crystals," arXiv: 2007.04875 (2020).
25. B. Xie, H. Wang, H. Wang, X. Zhu, J. Jiang, M. Lu, and Y. Chen, Phys. Rev. B **98**, 205147 (2018).
26. Y. Ota, F. Liu, R. Katsumi, K. Watanabe, K. Wakabayashi, Y. Arakawa, and S. Iwamoto, Optica **6**, 786 (2019).
27. X. Chen, W. Deng, F. Shi, F. Zhao, M. Chen, and J. Dong, Phys. Rev. Lett. **122**, 233902 (2019).
28. B. Xie, G. Su, H. Wang, H. Su, X. Shen, P. Zhan, M. Lu, Z. Wang, and Y. Chen, Phys. Rev. Lett. **122**, 233903 (2019).
29. L. Zhang, Y. Yang, Z. K. Lin, P. Qin, Q. Chen, F. Gao, E. Li, J. Jiang, B. Zhang, and H. Chen, Adv. Sci. **7**, 1902724 (2020).
30. Y. Chen, F. Meng, Y. Kivshar, B. Jia, and X. Huang, Phys. Rev. Res. **2**, 023115 (2020).
31. B. Xie, G. Su, H. Wang, F. Liu, L. Hu, S. Yu, P. Zhan, M. Lu, Z. Wang, and Y. Chen, Nat. Commun. **11**, 3768 (2020).
32. X. Zhou, Z. K. Lin, W. Lu, Y. Lai, B. Hou, and J. H. Jiang, Laser Photon. Rev. **14**, 2000010 (2020).
33. M. Xiao, Z. Q. Zhang, and C. T. Chan, Phys. Rev. X **4**, 021017 (2014).
34. W. A. Benalcazar, B. A. Bernevig, and T. L. Hughes, Phys. Rev. B **96**, 245115 (2017).
35. M. Galli, S. L. Portalupi, M. Belotti, L. C. Andreani, L. O'Faolain, and T. F. Krauss, Appl. Phys. Lett. **94**, 071101 (2009).
36. A. E. Miroshnichenko, S. Flach, and Y. S. Kivshar, Rev. Mod. Phys. **82**, 2257 (2010).
37. J. D. Joannopoulos, S. G. Johnson, J. N. Winn, and R. D. Meade, *Photonic Crystals: Molding the Flow of Light*, 2nd ed. (Princeton University, 2008).
38. K. Inoue, H. Oda, A. Yamanaka, N. Ikeda, H. Kawashima, Y. Sugimoto, and K. Asakawa, Phys. Rev. A **78**, 011805 (2008).
39. V. S. C. M. Rao and S. Hughes, Phys. Rev. B **75**, 205437 (2007).